CHAPTER 7

BUILDING DEPOSITIONAL SYSTEMS

In Chapter 1 we argued that interpreting the paleogeologic origin of a particular sedimentary sequence can be significantly aided by dynamic mathematical modeling. Here, we provide some illustrations, showing how modules discussed previously can be assembled into programs that simulate larger depositional systems. We then conduct sensitivity experiments using the programs to gain insight into the origin and character of river profiles and fluvial sequences in foreland basins.

RIVERS AND THEIR LONGITUDINAL PROFILES

The longitudinal profiles of many rivers are smooth and concave-upwards functions of exponential, logarithmic, or power form (Figure 7-1). It is commonly assumed that rivers of this type are graded, by which is meant that the river has achieved a mass equilibrium and is in a state of little additional morphometric change over time scales of thousands of years.

The early explanation for concave graded profiles, due to that giant of geology G. K. Gilbert (1877), is that bed slope is inversely related to local water discharge, because a larger discharge is accommodated by a larger ratio of cross-sectional area to wetted perimeter. This larger ratio provides a more efficient means of conveyance, thereby allowing a lesser energy slope. Because water discharge increases downstream as a power function due to lateral inflow from tributaries, slope decreases as a power function of distance downstream.

The situation is not that simple, however. Even in Gilbert's time, it was generally known that grain size decreases downstream in rivers (e.g., Sternberg, 1875), and depending upon which is cause and which is effect, we might argue that grain

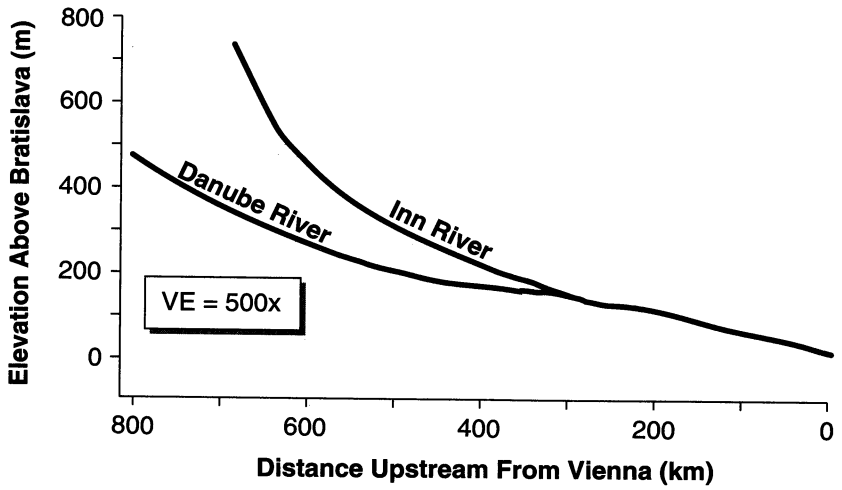

Figure 7-1 Two typical longitudinal profiles of rivers.

size controls profile concavity, too. In addition, many rivers are subjected to uplift or subsidence rates of millimeters per year, and also to varying rates of lateral sediment inflows. We can imagine that these also must play a role.

All of this is of interest to students of geomorphology and sedimentary geology because longitudinal profiles are often used as evidence for base level or climate changes in the past. Also, as mentioned in Chapter 1, many ancient fluvial deposits exhibit a decrease in grain size down the suspected paleoslope (see Figure 1-6, for example). Traditionally, this decrease has been used to define a distance back to the source terrain. But as the following analysis will show, these interpretations are probably not appropriate. Rather, the longitudinal profiles and downstream fining of streams provide information on the sediment- and water-discharge characteristics of the parent stream, the sediment yield of the source terrain, uplift rates in the source terrain, and subsidence of the basin.

Creating a 2-Dimensional River

To explore the origin of river profiles requires construction of a two-dimensional river with an erodible bed that responds to a tectonically active landscape. Therefore we must mathematically describe (1) gradually varied flow, (2) total sediment transport and associated processes such as settling of various sized grains, (3) tectonic uplift or subsidence, (4) conservation of the bed, and (5) sediment and water inflow to the stream. Modules for all these processes have been presented in previous chapters. Here they are linked together into a program called LONGPRO that is presented in Program 25. Within this program, it should be noted that the subroutine calculating the flow field, subroutine FLDTA, here contains a bisection algorithm to solve the gradually varied flow equation, whereas in Program 4 of Chapter 4, Henderson's method is used. The bisection method is less efficient, but more robust. Also the sediment-transport equation and bed conservation treatment are simpler than those presented in Chapter 4.

Constructing a Graded River

To construct a realistic graded river requires specifying the downstream increases in water and sediment discharge and width. As discussed in Chapter 3, geomorphological studies have shown that the lateral inflows per unit stream length of water q and sediment q_s are roughly independent of location. In the model LONGPRO, a lateral sediment inflow is treated as an increase in elevation of the bed in the bed-continuity equation. Therefore q_s values are multiplied by $\Delta t/W$, where W is calculated from (7-1).

Because our model is only two dimensional, it will not automatically calculate an equilibrium hydraulic geometry at each cross section. Therefore, we also must specify a spatial change in channel width. In dimensionless form, this is:

$$\frac{W}{W_{max}} = \left(\frac{Q}{Q_{max}}\right)^{p} \qquad \textbf{(7-1)}$$

where: p = 1/2 for mean annual discharges of rivers in eastern United States.

In addition, we need to specify an initial longitudinal profile. This will either be a monotonically decreasing form, or, in the interests of keeping the time to equilibrium short, an exponential function of the form:

$$y = y_0 exp\,(-k) \qquad \textbf{(7-2)}$$

where: k = constant greater than zero.

Equations (7-1) and (7-2) are programmed in subroutine SETUP of Program 25.

The Roles of Discharge and Sediment Input

We first explore the influence of sediment input on the longitudinal profile of a stream. Consider a river everywhere flowing over alluvium of 2 mm grain size. Its profile at time zero starts at 4000 m in the headwaters, and drops to 3970 m over 100 km. Maximum discharge at the downstream end is 100 $m^3\ s^{-1}$, where the maximum width is 50 m. The downstream boundary condition for the flow is a temporally constant water surface elevation of 3975 m. The input file is presented in Table 7-1.

Experiment 7-1: River Profile Graded to Steady Sediment Supply

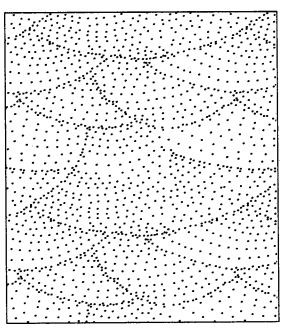

Experiment 7-1 starts with a flat reach of slope 0.0003 subject to a steady uniform discharge of 100 m^3/s in a rectangular channel of constant width of 25 m. Sediment of uniform size equal to 0.002 m diameter is fed into the upstream end of the reach at a temporally constant rate of 100 kg/s. No sediment or water enters the reach from its sides. The computed bed and water depths evolve as illustrated in Figure 7-2. As expected, alluviation occurs upstream at high rates initially. The bed slope steepens and finally comes to grade at a slope that is just adequate to transport the imposed sediment feed, in this case a slope of 0.0016. Notice how the water depth starts at about 4.25 m and evolves to a uniform depth of about 2.25 m.

Table 7-1 Sample input file for Program 25.

```
RUN NAME FOR PLOT FILES (A4):
tst1
LENGTH OF REACH (KM) (RLONG) <100. >
DISTANCE BETWEEN NODES ALONG REACH (KM) (DELX) < 1.0 >
TIMESTEP (HRS) (DELT) < 24.00 >
NUMBER OF TIMESTEPS < 876000>
RESULTS ARE PRINTED AT (XPRINT) DISTANCE INTERVALS (KM) < 1.0 >
RESULTS ARE PRINTED AT (TPRINT) TIME INTERVALS (HRS) < 43800.0>
MEDIAN GRAIN SIZE (DIMID) (M) < 0.002 >
RUN TITLE (A25):
rls: foreland test # 3/92
ELEVATION OF THE WATER SURFACE AT THE CONTROL NODE (M) < 3975.0 >
SLOPE OF INITIAL RIVER BED < 0.0003 >
QMAX at XMAX (m**3/sec) < 100.0 >
MAINNING N (SI UNITS) < 0.04 >
FACTOR BY WHICH SEDIMENT CONC'S ARE TO BE Adjusted < 1.0 >
INITIAL ELEVATION AT x=0 (M) < 4000.0>
TURN ON LOADING AT TIMESTEP: < 600000>
TURN OFF TECTONICS AT TIMESTEP: < 600000>
TURN ON TECTONICS AT TIMESTEP: < 600000>
TURN OFF TECTONICS AT TIMESTEP: < 600000>
NODE ALONG X AXIS AT WHICH TECTONIC ELEV CHANGES START < 1>
RATE AT WHICH THE ELEV DUE TO TECTONICS CHANGES < 0.0 >
SEDIMENT CONCENTRATION OF LATERAL INFLOW (PROPORTION) < 0.000 >
MASS FEED RATE AT UPSTREAM BOUNDARY (KG/S) < 100.0 >
```

Figure 7-2 Plot of computed bed elevations and water depths for Experiment 7-1 (A and B) and Experiment 7-2 (C and D). Each line represents 10 years.

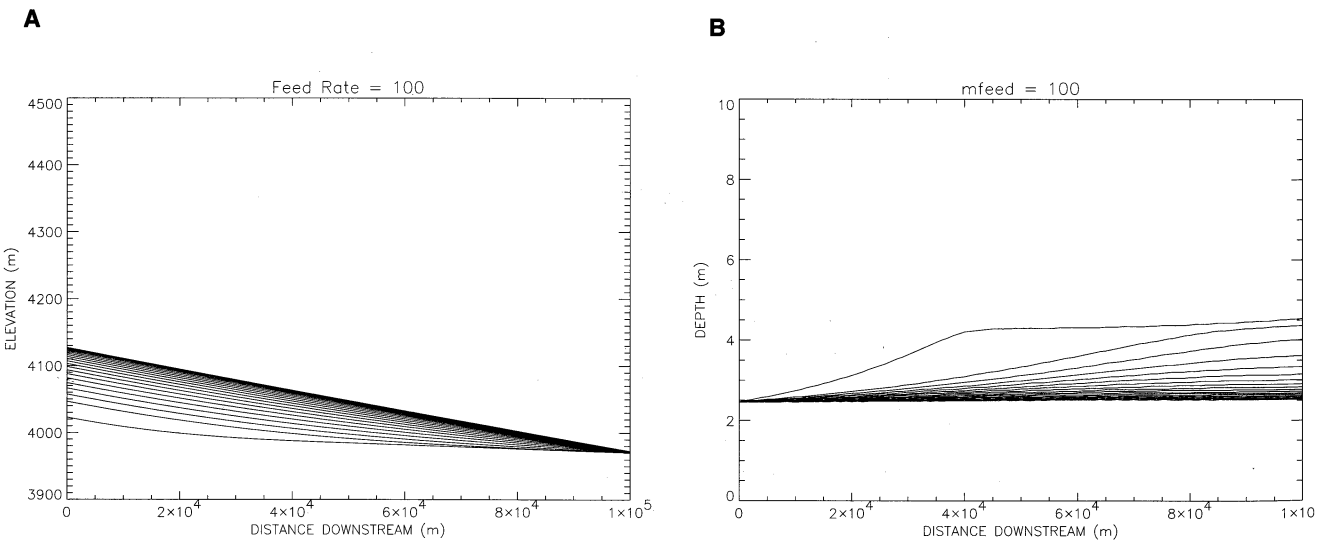

Experiment 7-2: River Profile Graded to Doubled Steady Sediment Supply

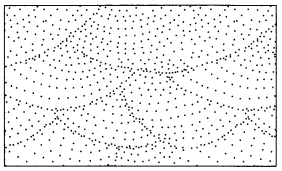

Experiment 7-2 starts with the same conditions as Experiment 7-1, but the feed rate is doubled. Again the stream evolves to a new uniform slope, in this case 0.00283. Notice that a doubling of the feed rate does not lead to a doubling of the graded slope because the sediment transport rate is a high-order power of bed-shear stress (which is linearly proportional to slope).

Experiment 7-3: River Profile Graded to Nonuniform Discharge

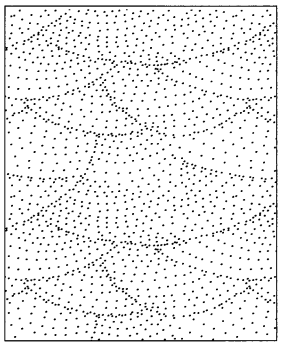

In Experiment 7-3 the discharge increases linearly downstream according to the rule:

$$Q = Q_{max}\, jn/m \tag{7-3}$$

where: m = maximum number of nodes

jn = node number.

Width also increases downstream, but nonlinearly according to the rule width = $\text{width}_{\max}\sqrt{\frac{Q}{Q_{max}}}$, a relationship justified earlier. Again the feed rate is 200 kg/s at the head of the reach. As can be seen in Figure 7-3, the graded profile is now concave, with water depths increasing downstream. The origin of this shape can be best understood by analyzing the sediment transport equation, in this case Yang's total load formula (4-72). Because the stream is at grade, then by definition all of the sediment fed at the head must be transported through the reach at the feed rate. That means the spatial gradient of sediment transport rate must equal zero. Inspection of Yang's equation shows that this can happen only if an increasing discharge is exactly balanced by an increasing width and decreasing slope. Apparently, in this case the prescribed increase in width cannot do the job alone, and the slope decreases to keep the sediment transport rate constant along the stream.

C

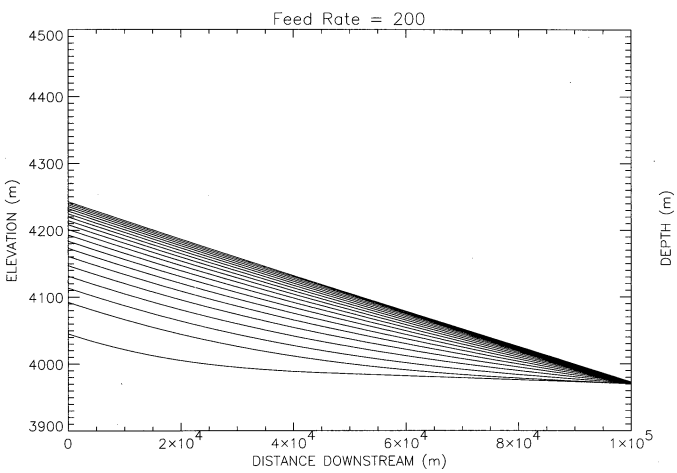

D

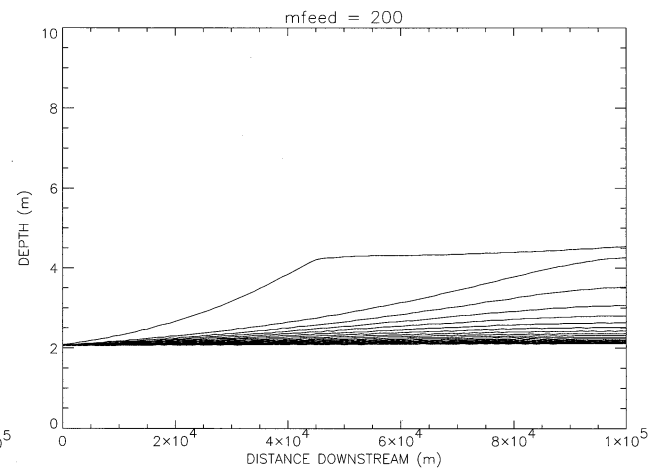

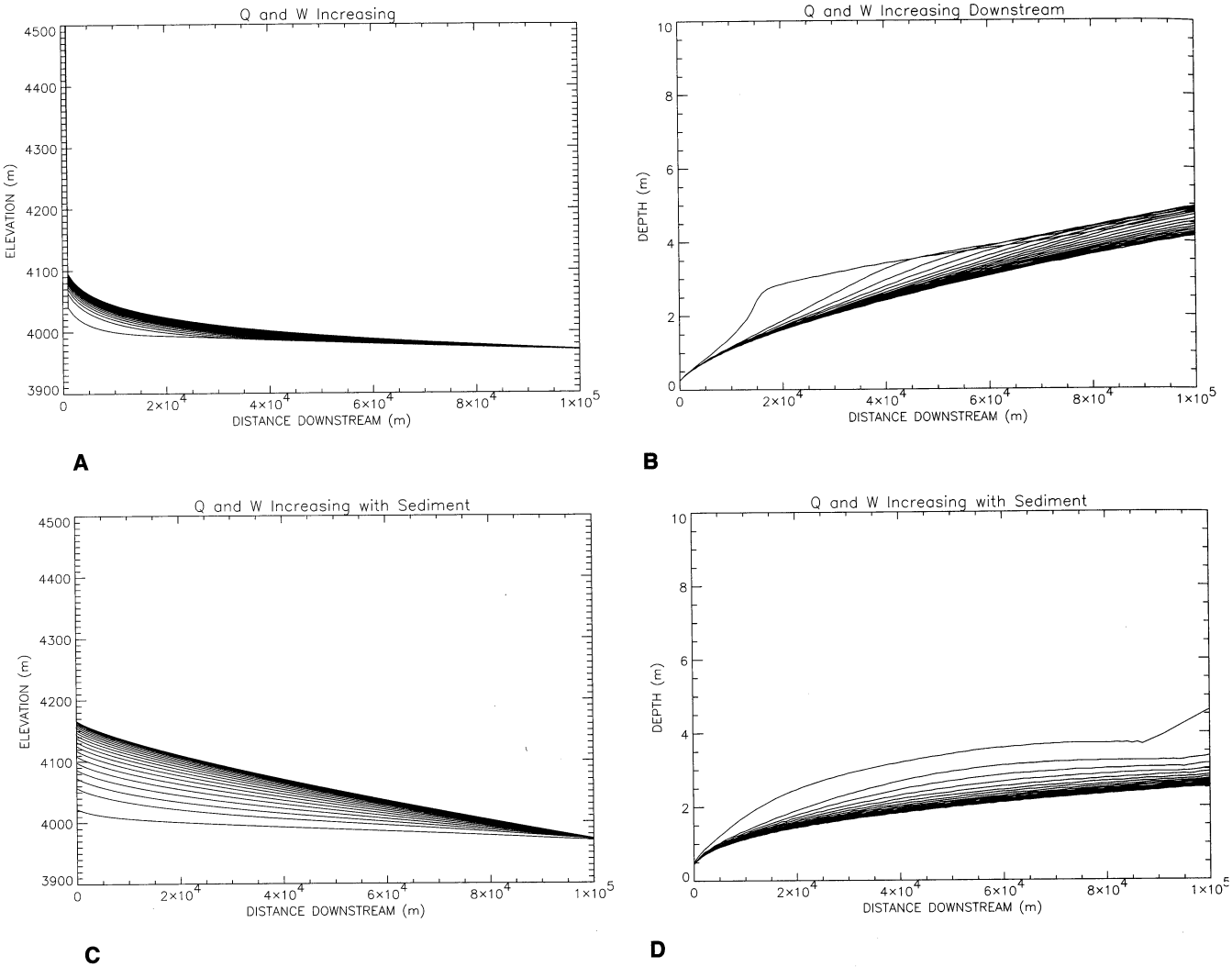

Figure 7-3 Plot of computed bed elevations and water depths for Experiment 7-3 (A and B) and Experiment 7-4 (C and D). Each line represents 10 years.

Experiment 7-4: River Profile Graded to Nonuniform Sediment and Water Supply

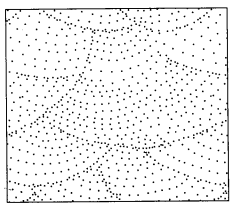

Experiment 7-4 is the same as Experiment 7-3 except that the sediment feed at the head is turned off and lateral feed is turned on by setting *sedcon* = 0.0005 in Table 7-1. As mentioned earlier, lateral feed is represented in the model by adding sediment to the bed. The relationship is given by:

$$Q_{in} = sedcon\,(q_{jn} - q_{jn-1})\,\frac{\Delta t}{W_{jn}\Delta x} \qquad \textbf{(7-4)}$$

where: Q_{in} = amount of lateral sediment feed at node *jn* that enters over timestep Δt,

q = water discharge,

W = stream width.

Q_{in} is proportional to the amount of water that enters laterally at node *jn*. Remember that the volume of water entering from the side per unit stream length is a constant that is independent of position along the channel, such that stream discharge increases linearly with distance downstream. Therefore, the amount of sediment entering is constant from node to node, similar to many real streams, as justified in Chapter 3. The results (Figure 7-3) show that the equilibrium slope is slightly concave. The magnitude of the concavity depends upon the balance between the rates at which discharge and sediment input increase downstream. We can conceive of a case where the profile is convex upwards because the sediment flux to the channel imposes a load which the increasing discharge cannot carry, thereby requiring an ever increasing slope at downstream sites.

Experiment 7-5: River Profile Graded to Nonuniform and Lesser Sediment and Water Supply

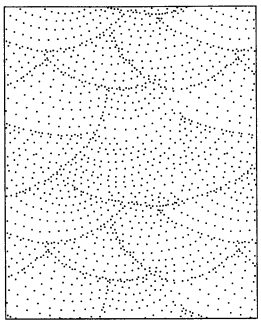

Experiment 7-5 is the same as Experiment 7-4 except the amount of sediment entering laterally is cut in half. Results (Figure 7-4) show that the slope of the graded profile is roughly reduced by half while maintaining its subtle concavity.

Role of Tectonics

Next we turn our attention to the roles uplift and subsidence play in controlling the graded profile of a river. Our base line will be Experiment 7-1. To it we will add a temporally constant tectonic rotation about a hingeline located at the downstream end of the reach at *jn* = *m*. The line of FORTRAN code in Program 25 that accomplishes this is:

```
ELEV(1) = ELEV(1) + RATE*(M - I + 1)
```

(7-5)

where: RATE = 0.001.

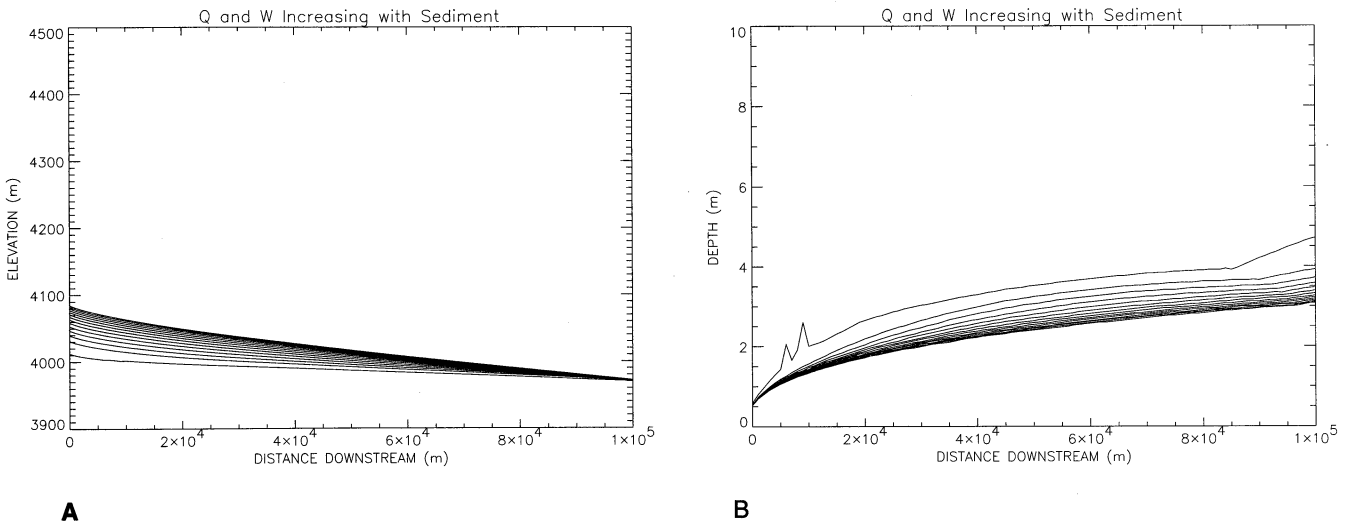

Figure 7-4 Plot of computed bed elevations (A) and water depths (B) for Experiment 7-5. Each line represents 10 years.

Thus 1.01 cm of elevation is added to the first node every timestep, 1.00 cm to node 2, and so on decreasing to zero cm added to node m.

Experiment 7-6: River Profile Graded to a Tectonic Rotation

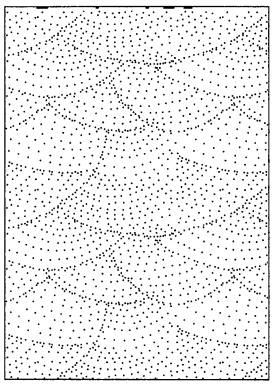

As Figure 7-5 shows, the stream profile steepens through time, passing through a concave and then constant slope stage. The graded profile, obtained after about 300 years, is convex upwards. The explanation for this shape is contained in the equation for conservation of the bed (4-70) of Chapter 4 modified to accommodate introduction of sediment into the channel by uplift:

$$\sigma_j(1-p)\frac{\partial}{\partial t}(bz_{b_{ij}}) + \frac{1}{g}\frac{\partial}{\partial x}(bi_{b_{ij}}) + \frac{\partial}{\partial x}(S_{s_{ij}}) - q_s = 0 \qquad \textbf{(7-6)}$$

where: σ_j = density of jth grain species,
p = bed porosity,
b = width of active bed, assumed to be equal to flow width,
$z_{b_{ij}}$ = bed elevation attributable to ith-jth bed fraction,
$i_{b_{ij}}$ = bedload transport rates of ith-jth fraction (kg s^{-3}),
$S_{s_{ij}}$ = suspended load transport rates of ith-jth fraction (kg s^{-1}),
q_s = rate at which sediment enters river bed from beneath as consequence of uplift.

Henceforth, the i and j subscripts will be dropped because we treat only one grain size and type.

At grade, there will be no temporal change in bed elevation, and (7-6) may be written as:

$$\frac{\partial}{\partial x}\left(\frac{1}{g}bi + S_s\right) = q_s \qquad \textbf{(7-7)}$$

This equation says that the local spatial gradient in sediment flux must match the local uplift mass flux into the channel. The latter is highest at the upstream end and decreases linearly downstream. Now, what controls the spatial gradient in

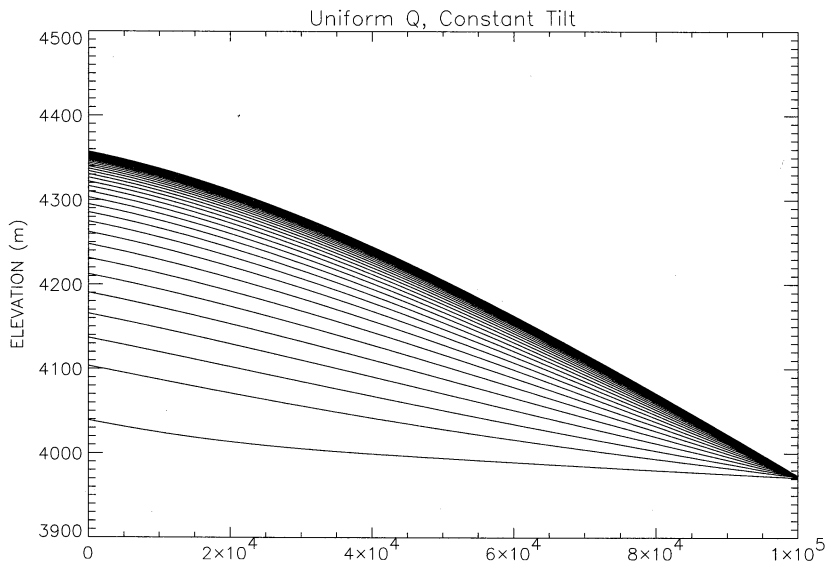

Figure 7-5
Model results for Experiment 7-6, a case of constant angular rotation about control node causing linearly increasing uplift upstream.

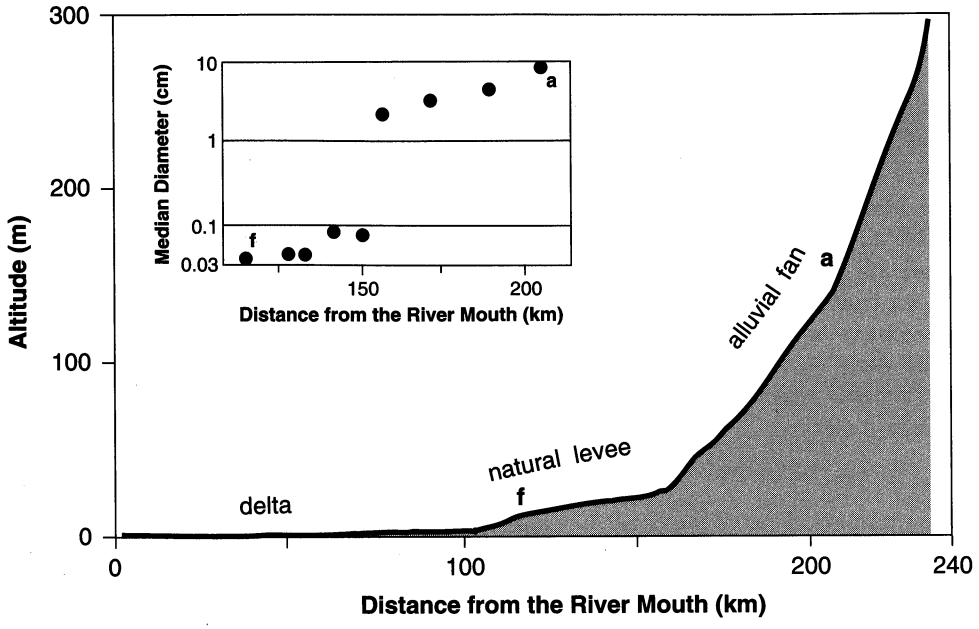

Figure 7-6
Longitudinal profile and sediment characteristics of the Kinu River, Japan (from Ohmori, 1991, after Yatsu).

sediment flux? It is the spatial gradient in bed-shear stress and velocity, and hence at constant discharge, the spatial gradient in bed slope. A spatial gradient in bed slope is a curvature. Therefore, we conclude that because uplift mass flux is greater upstream, curvature must also be greater upstream. But why is the curvature convex upwards, rather than concave? The answer is that clear water is entering the reach at its upstream end. To satisfy the transport capacity of the stream, sediment is eroded from the first few nodes at a high rate. Downstream nodes must transport this sediment, *plus* sediment entering from beneath due to uplift. Therefore, local slopes downstream must be higher.

Role of Grain Size

Consider field data from the Kinu River of Japan (Figure 7-6). The Kinu is typical of many rivers. It possesses a characteristic concave profile and a bed texture that becomes finer downstream, albeit not in a straightforward manner. Median diameter of the bed drops by more than an order of magnitude when passing from the alluvial fan to the reach with natural levees, a behavior characteristic of many rivers (Parker, 1991). Nevertheless, within each geomorphic setting, a systematic downstream fining is evident. Because of its tectonic setting, the Kinu receives sediment at rates of 100 to 2000 $m^3/km^2/yr$ that are some of the highest in the world. In many ways it is logical to view the Kinu as a modern analog of the ancient river systems that drained off ancient orogens into foreland basins, such as those that created the Mississippian Pocono Formation of the central Appalachians (Figure 1-6). But before attempting to infer the longitudinal profile of Pocono rivers from their clast sizes, we need to better understand the origin of the Kinu's profile and texture in our attempt to separate cause and effect.

An exhaustive treatment of the interplay between grain size and river longitudinal profile would require using the complete heterogeneous total load transport model of Chapter 4. Here we choose a simpler route for illustrative purposes, and treat grain size decreases downstream that arise solely from comminution. That comminution exists is well documented (cf. Parker, 1991), at least for the gravel

fraction. Almost certainly some of the size decrease in Figure 7-6 is due to more rapid and higher volume transport of finer grains. But strictly speaking, in the absence of comminution, a stream at grade must pass each size fraction at the rate each fraction enters the stream. If one assumes that the alluvium underlying the mobile population contains the same size distribution as the mobile population, then it follows that the truly graded stream in the absence of comminution *will not become finer downstream.* Therefore, our assumption of comminution without differential transport by size is, at minimum, theoretically sound.

For simplicity, we assume a gravel-bed stream in which each clast loses volume according to a first-order rate law proposed by Kuenen (1956):

$$D = D_o e^{-\beta x} \tag{7-8}$$

where: D = grain diameter,
β = comminution coefficient in terms of fraction lost per unit distance traveled,
x = distance traveled.

If no sediment enters laterally, then each downstream site sees only one grain size. Program 25 is easily modified to simulate this effect by inserting the following lines in Subroutine ERODEP at the start of the space loop:

```
DIMID = 0.01*DEXP(-1.18812E-05*JN*DELX)
CALL SETTLE
```

Experiment 7-7: River Profile Graded to a Downstream Decrease in Grain Size

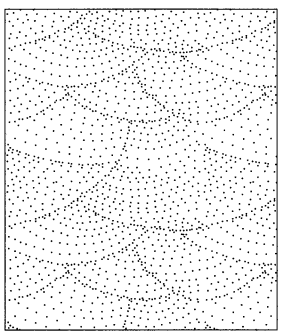

Consider a river with boundary initial conditions as posed in Experiment 7-1, to which is added a decrease in downstream grain size as discussed above, where the grain size at node 1 is 10 mm and β equals 1.18812×10^{-5}. The resulting graded profile and approach to grade are presented in Figure 7-7.

The profile is concave upwards and much steeper than the profile of Experiment 7-1. The concavity arises because steeper slopes are required to pass the imposed sediment load when it is composed of 10-mm clasts, such as at node 1, than when it is composed of 0.3-mm grains as at node 101. Even though the mass flux of grains remains constant through the reach (at the feed rate), the stream requires a lower slope to pass the load when it is finer.

RIVERS IN FORELAND BASINS AND THE SEQUENCE STRATIGRAPHY OF THEIR DEPOSITS

Predicting lateral facies variability and reservoir architecture of coastal plain fluvial facies requires mapping "high-frequency" sequence boundaries and associated lowstand facies, an important point well illustrated by the Exxon Group (Van Wagoner et al., 1990; Van Wagoner et al., 1991). Sequence boundaries, in the new terminology of sequence stratigraphy, are regionally extensive surfaces separating one relatively conformable, genetically related succession of strata from another. Typically, they are unconformities. "High frequency," in this context, means on the order of 10^5 years. In the subsurface, where the available data are never complete enough and where log and seismic signatures are often ambiguous, mapping sequence boundaries is aided by comparing the strata of interest to well-known

analogs. These are often modern deposits, such as along the Gulf Coast, or well-exposed ancient deposits.

Two such ancient deposits of particular note are the Campanian-age Blackhawk and Price River Formations in the Book Cliffs region of east-central Utah. These strata are superbly exposed, thereby offering an unparalleled opportunity to examine nearshore marine sequence boundaries and lowstand facies along a proximal foreland shoreline (Van Wagoner, 1991; Taylor and Lovell, 1991). As documented by the Exxon Group and earlier workers (Young, 1957; Balsley and Horne, 1980; Newman, 1985; Swift et al., 1987; Franczyk, 1989), they consist of numerous littoral sandstone tongues which extend eastward or southeastward from intercalated sandstones, shales, and coals of the alluvial plain into the marine Mancos Shale. Sequence boundaries within these units are defined as regionally extensive surfaces of truncation, above which is a marked basinward shift in facies.

In the lower and upper Sego Sandstones of the Price River Formation, and the Anchor Tongue of the Mancos Shale, Van Wagoner (1991) recognizes nine such sequence boundaries (Figure 7-8). Based on ammonite dating, the intervening sequences were deposited over an interval no greater than 1.2 million years, making each of roughly 150,000 years duration. Each sequence boundary is thought to have been formed by fluvial incision during a relative fall in sea level.

The amount of fall is not specified, but insofar as fluvial incision occurs in mudstones of the lower shoreface and offshore transition, the magnitude must be on the order of tens of meters. Similarly, sandstones of the Blackhawk Formation's Kenilworth Member are interpreted by Taylor and Lovell (1991) to form parts of two high-frequency sequences, although the exact durations of the sequences are not specified. Based on the amount of fluvial channel incision at the

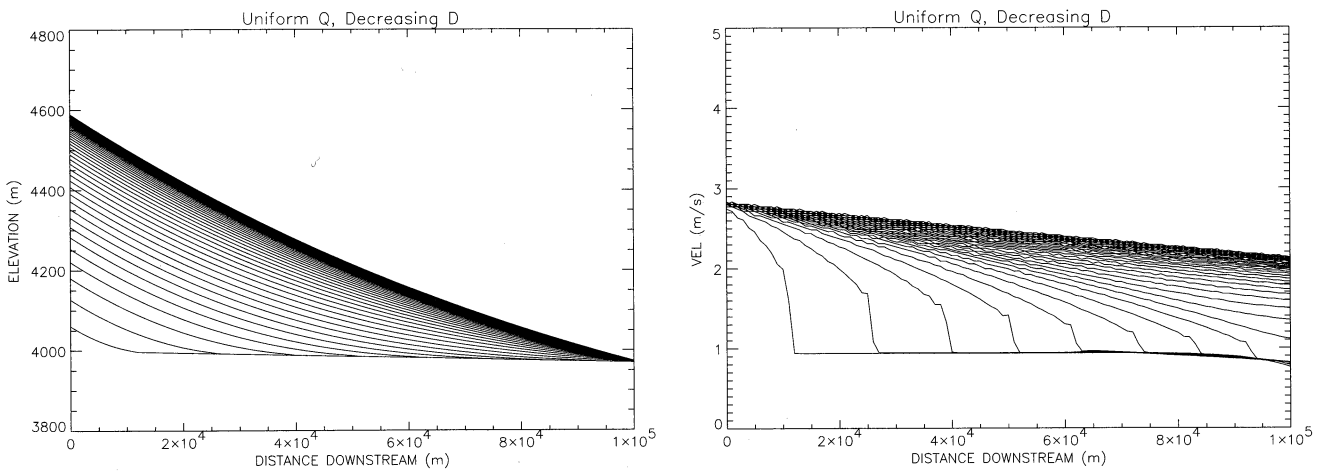

A B

Figure 7-7 Model results for Experiment 7-7, a case of steady uniform discharge, sediment feed rate of 100 kg/s at head, and downstream reduction in grain size due to comminution. (A) Longitudinal profiles every 20 years; (B) Stream velocities every 20 years.

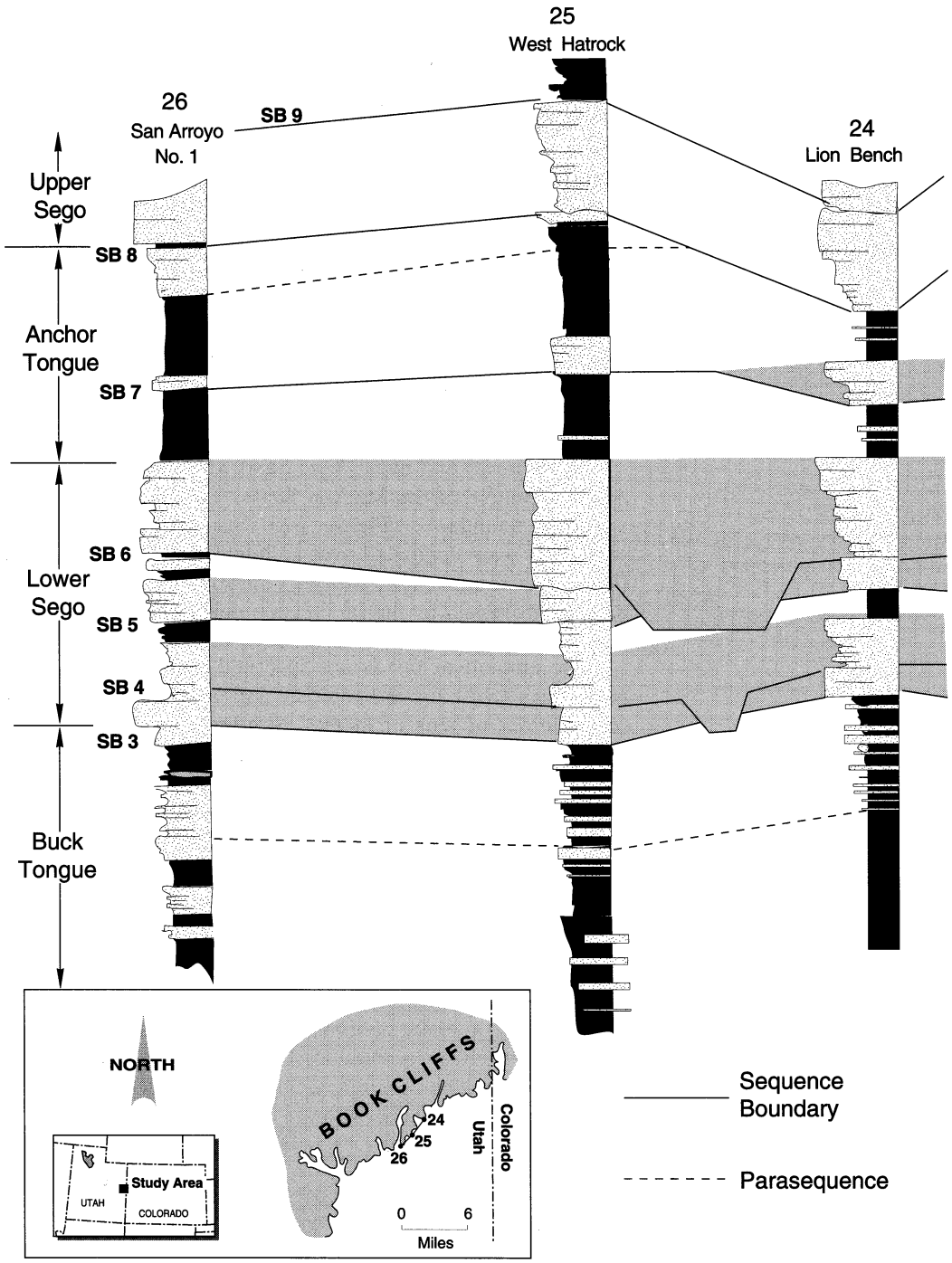

Figure 7-8 Measured stratigraphic sections of Lower and Upper Sego Sandstones of Price River Formation, Book Cliffs, Utah, showing high-frequency sequence boundaries. Gray stippling denotes estuarine valley fill sequences. Remainder of sections are composed of black marine mudstones and shoreface sandstones. (From Van Waggoner, 1991.)

sequence boundary, the relative sea level fall is estimated by them to be at least 60 feet.

Implicit in the logic of using the Blackhawk and Price River Formations as analogs, is the assumption that the origin of their sequence boundaries is a well-understood function of such initial and boundary conditions as eustatic sea level changes, local subsidence, uplift in the source, and climate. For only then could one generalize the geometries and facies relationships of these rocks to different basin settings.

Unfortunately, the origin of these sequence boundaries is not well understood. The Exxon Group has hypothesized that the sequences they have so nicely documented result from "minor high-frequency sea-level falls...(wherein) only the center of the basin would contain water" (Van Wagoner, 1991). To the best of our knowledge, no mechanism other than glacio-eustatic has been proposed for sea level fluctuations of this magnitude at the periodicity of about 100,000 years. Van Wagoner's hypothesis thus implies that some permanent alpine and polar ice existed in the Cretaceous. But paleoclimate indicators such as paleobotanical data collected from near the poles and isotope-derived sea surface temperatures indicate that the Cretaceous was a period of unique warmth, with little if any polar ice (E. Barron, pers. com.). This is a problem.

Furthermore, we do not yet know, from a theoretical point of view, what degree of fluvial incision to expect from a sea level drop of this magnitude. In fact, Posamentier and Vail (1988) argue that rivers aggrade during relative sea level fall (p. 135). While seemingly absurd at first glance, it is probably a theoretically admissible solution. Also, we have as yet not considered the role that a fluctuating sediment supply might play. Changes in interior continental climates are now known to occur due to changes in solar insolation. Changes in solar insolation arise from periodic changes in earth's orbital parameters, a phenomenon first discovered in 1920 by Milutin Milankovitch, a Yugoslavian mathematician. Thus, periodically changing climates could vary the weathering rate and hydrology of the Sego source terrain, producing cut and fill cycles with roughly the same period as expected for glacio-eustatic sea level fluctuations. Until these issues are explored, the full significance of the field relationships cannot be understood.

It is precisely in these cases where modeling can help. Here, we modify the two-dimensional river model of the previous section to include flexure and varying sea level, and conduct numerical experiments to test the following three hypotheses:

1. The Sego sequences result from glacio-eustatic sea level fluctuations.
2. The Sego sequences reflect variations in the rate of mass flux into the source terrain. These variations alter the rate of basin subsidence through crustal loading as well as the rate of sediment supply through changing relief.
3. The Sego sequences are the product of sediment supply variations resulting from Milankovitch-scale climate change.

While it is difficult to conceive of crustal deformation operating at these high-frequency time scales, we include the second hypothesis for completeness.

Coupling the 2-D River and Elastic Flexure Models

The model consists of a source terrain and a single thread river of known discharge and width carrying sediment eroded off the source to a basin of specified initial depth, with the elastically deforming lithosphere responding to tectonic and

sedimentary loads. The source terrain provides the initial supracrustal load that creates the basin, the initial slope of the river, and a sediment load the river must carry. The river builds an alluvial plain and aggrades the continental shelf into a standing body of still water of specified, temporally variable, surface elevation.

LONGPRO (Program 25) of the previous section provides a convenient starting point. To it is added Subroutine FLEX (Program 1) presented in Chapter 2, simulating elastic flexure, and a new subroutine, EUSTACY, presented in Program 26, called to set the downstream boundary condition of water surface elevation. The complete program, called FILLER, is included on the diskette.

The Role of Eustacy

To test the first hypothesis we hold sediment feed, water discharge, and tectonics constant, while varying sea level according to some simple functions. In this manner we can determine the depth and extent of fluvial incision as a function of sea level shifts (both horizontally and vertically) and rate of aggradation or subsidence.

Experiment 7-8: River Progradation with Constant Base Level

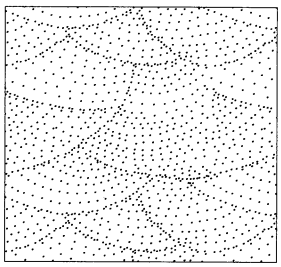

The first experiment starts with a plane sloping from 4000 m to 3700 m, no subsidence, and a temporally constant sea level at 3975 m. It is Experiment 7-1 of the previous section repeated with a steeper slope, such that the river now flows into a standing body of water. Results (Figure 7-9) show that unlike Experiment 7-1, here progradation of the river mouth causes continuous alluviation of the river. Only when the basin has filled across to the control reach does the river come to grade. This suggests that even in the absence of sea level change, rivers alluviate along their middle and lower courses during regression.

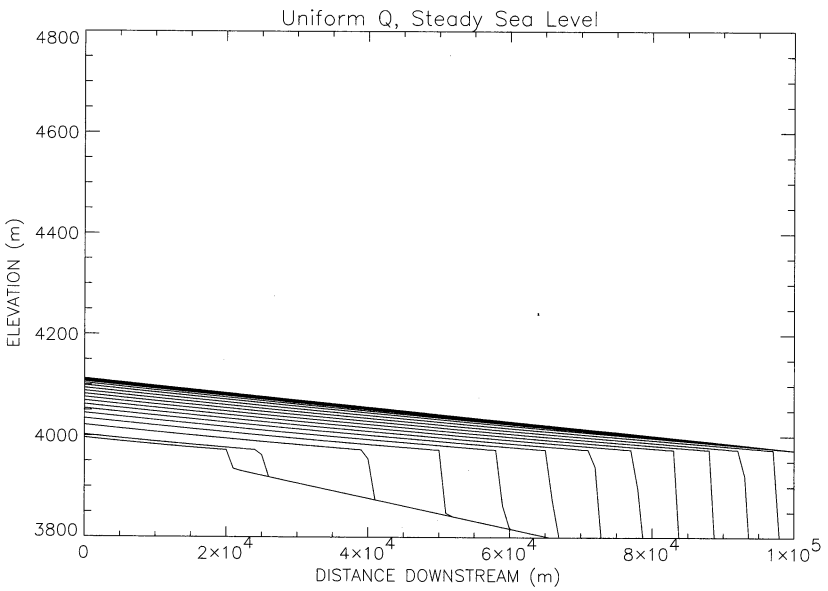

Figure 7-9 Model results of Experiment 7-8, where river of uniform discharge flows into standing body of water with constant sea level.

Interestingly, the profile of the aggrading river is almost identical to the final graded profile.

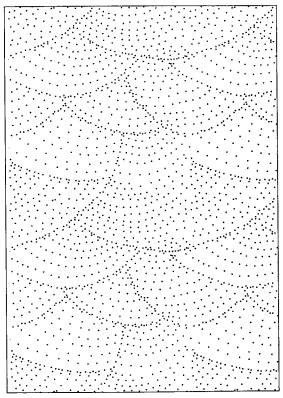

Experiment 7-9: River Progradation with Variable Base Level

In this experiment, the same boundary and initial conditions are applied (Table 7-2), except sea level is varied according to the simple sine function (expressed in FORTRAN notation):

$$WSEBC = WSEBCB + AMP*DSIN(6.28319*NT*DELT/T) \quad (7\text{-}9)$$

where: WSEBC = water surface elevation boundary condition at control node,
WSEBCB = mean water level (3975 m) of previous run,
AMP = amplitude of variation (30 m),
T = period (50 years).

Results are shown in a cross section (Figure 7-10) and a space-time diagram (Figure 7-11) where bed elevation is plotted as a function of distance downstream and of time. Throughout the duration of the run, a delta builds across the initial

Table 7-2 Input data file for Experiment 7-9

RUN NAME FOR PLOT FILES (A4):
RUN7
LENGTH OF REACH (KM) (RLONG) <100. >
DISTANCE BETWEEN NODES ALONG REACH (KM) (DELX) < 1.0 >
TIMESTEP (HRS) (DELT) < 24.00 >
NUMBER OF TIMESTEPS < 200000>
RESULTS ARE PRINTED AT (XPRINT) DISTANCE INTERVALS (KM) < 1.0 >
RESULTS ARE PRINTED AT (TPRINT) TIME INTERVALS (HRS) < 4380.0 >
MEDIAN GRAIN SIZE (DIMID) (M) < 0.001 >
RUN TITLE (A25):
Sine sea level curve, with RUN 1 conditions
ELEVATION OF THE WATER SURFACE AT THE CONTROL NODE (M) < 3975.0 >
SLOPE OF INITIAL RIVER BED < 0.003 >
QMAX at XMAX (m**3/sec) < 100.0 >
MAINNING N (SI UNITS) < 0.04 >
FACTOR BY WHICH SEDIMENT CONC'S ARE TO BE Adjusted < 1.0 >
INITIAL ELEVATION AT x=0 (M) < 4000.0>
TURN ON LOADING AT TIMESTEP: < 600000>
TURN OFF TECTONICS AT TIMESTEP: < 600000>
TURN ON TECTONICS AT TIMESTEP: < 600000>
TURN OFF TECTONICS AT TIMESTEP: < 600000>
NODE ALONG X AXIS AT WHICH TECTONIC ELEV CHANGES START < 1>
RATE AT WHICH THE ELEV DUE TO TECTONICS CHANGES < 0.0 >
SEDIMENT CONCENTRATION OF LATERAL INFLOW (PROPORTION) < 0.000 >
MASS FEED RATE AT UPSTREAM BOUNDARY (KG/S) < 100.0 >
AMPLITUDE OF SEA LEVEL SINE CURVE (M) < 30.0 >
PERIOD OF SEA LEVEL SINE CURVE (YRS) < 50.0 >

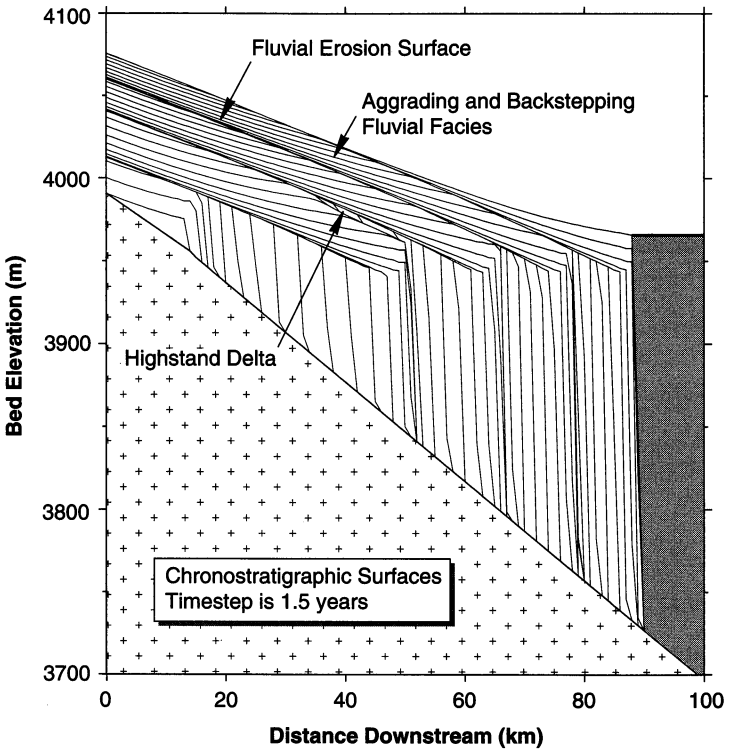

Figure 7-10
Modeled chronostratigraphic surfaces for a fluvial system subject to the boundary conditions of Experiment 7-9.

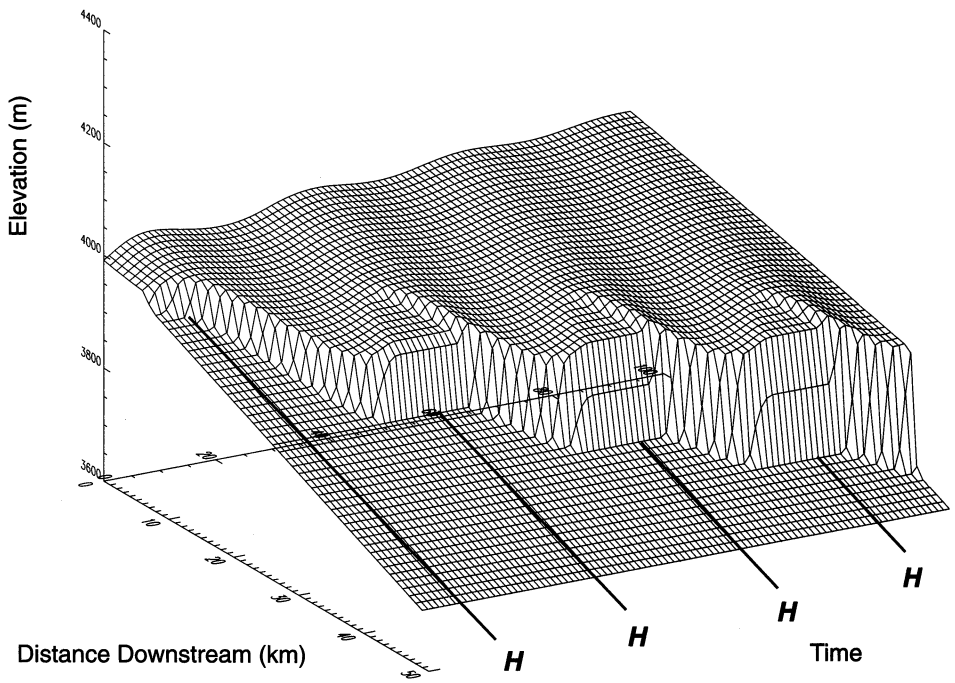

Figure 7-11
Model results for Experiment 7-9 where sinusoidal sea level causes scour and fill of constant discharge stream. This is a space-time diagram where H marks times of high sea level.

sloping plane, while the river aggrades up-river in its attempt to attain a graded profile. Superimposed on this general pattern are cut-and-fill cycles due to sea level variations. As sea level rises, progradation slows and then stops as sediment is trapped upstream, elevating the streambed there. As sea level begins to fall, a smaller delta builds out across the drowned subjacent delta as the river continues to alluviate upstream. Continued sea level fall initiates downcutting of the lower reach, removing this smaller delta, and its sediment is transported further downstream where it creates another advance of the main delta. Thus it is clear that the Sego sequence boundaries could be formed by similar sea level variations.

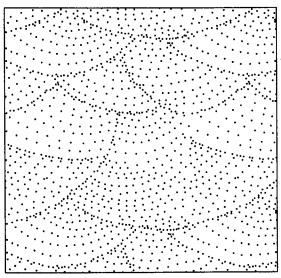

Experiment 7-10: River Progradation with Flexure and Constant Base Level

To test the second hypothesis, flexure will be turned on while keeping the initial and boundary conditions roughly similar to those in Experiment 7-8. Here, the initial slope is an order of magnitude greater and the water surface elevation is 175 m lower. The flexural rigidity is set to 2.4 x 10^{21} Nm, a value representing weak crust.

Results are presented as deflections of the original sloping plane (A) and bed surface elevations (B) in Figure 7-12. As sediment is eroded off the upland (from 0 to 4 x 10^4 m downstream), the crust flexes upwards through time, helping to

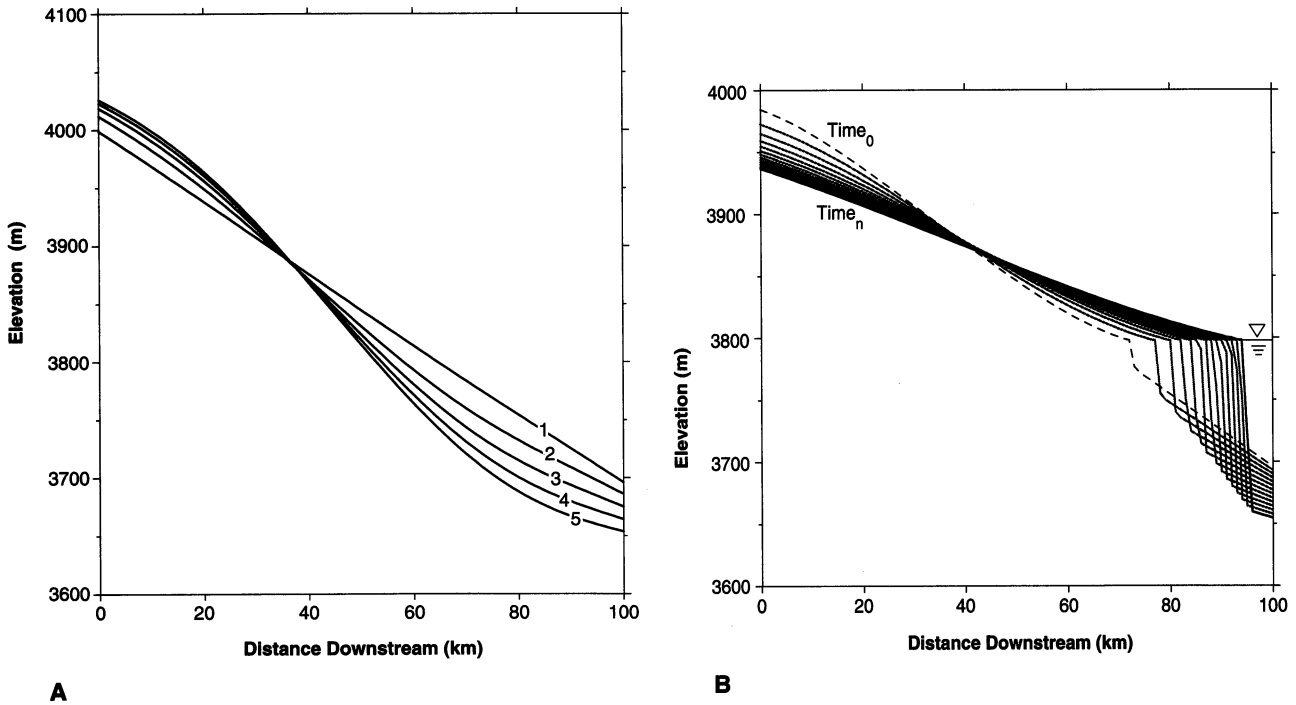

Figure 7-12 Computed results for Experiment 7-10 in which flexure of weak crust occurs in response to stream erosion in headwaters and deposition in a basin. (A) Flexural deformation of initial surface. Profiles 1-5 represent 1/2, 5, 10, 15, and 20 years, respectively. (B) Bed profiles over first 20 years of experiment. Early profiles are not migrated as flexure proceeds.

feed additional material to the stream. The eroded sediment is deposited in an adjacent sea where it flexes the crust downward, rapidly at first but then more slowly as the stream slope diminishes and less sediment is deposited per unit time (Figure 7-12 B). The position of the cross-over point, where erosion changes to deposition, is determined by the flexural rigidity of the crust and the sediment feed rate.

Experiment 7-11: River Progradation with Lesser Sediment Supply

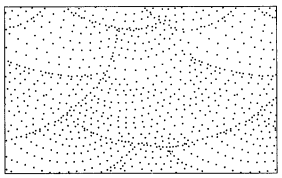

Reducing the feed rate by an order of magnitude in Experiment 7-11 (Figure 7-13) causes more erosion of the bed in the upland and therefore more flexure. The profile of the stream is convex up in the upland area because clear water enters at $x = 0$ and uplift rates are lower there than further downstream. Therefore, the stream can maintain the required sediment transport rate at a lower slope.

Role of Climate

To test the third hypothesis, sea level is held constant while varying sediment feed and water discharge. Ranges of sediment and water discharges can be estimated roughly from Cretaceous paleoclimate simulations by Glancy et al. (1986), Oglesby and Park (1989), and E. Barron (pers. com.), coupled with modern estimates of sediment yield as a function of relief and climate. These investigators

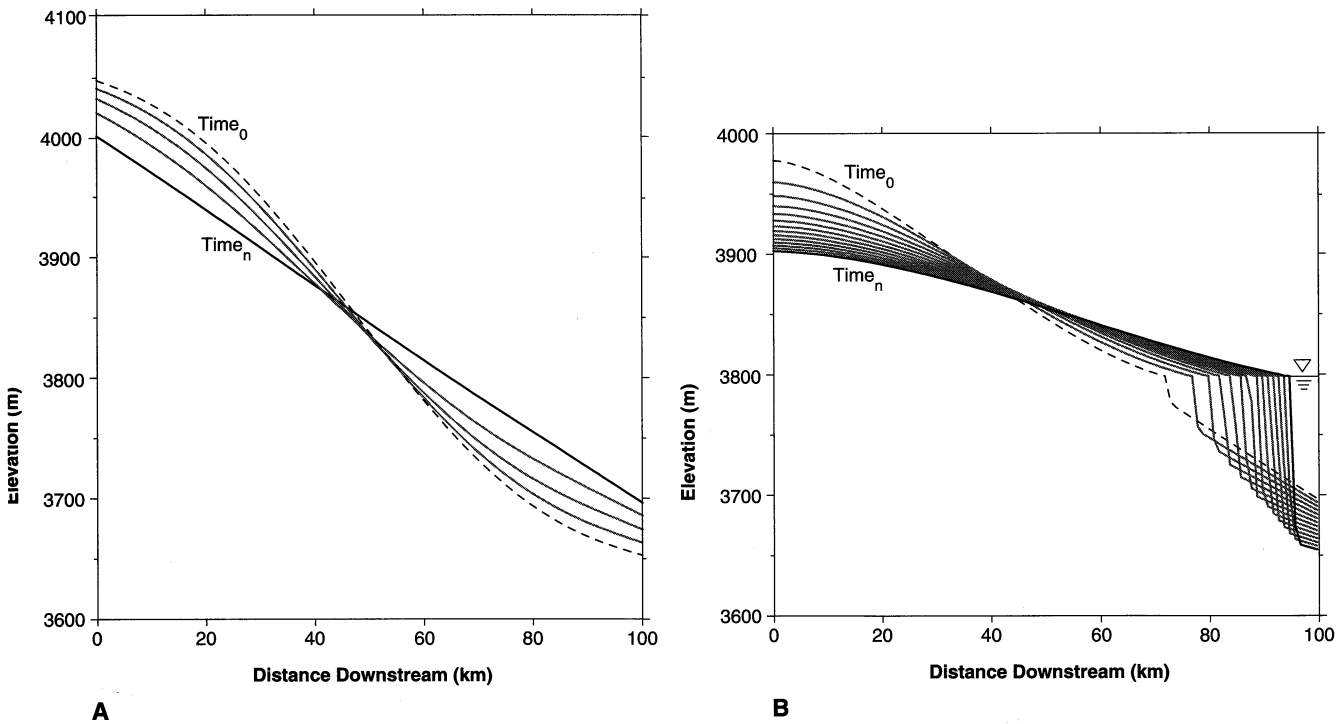

Figure 7-13 Results from Experiment 7-11 where sediment feed rate is reduced by an order of magnitude. (A) Flexural deformation of initial surface. Profiles 1 to 5 represent 1/2, 5, 10, 15, and 20 years, respectively. (B) Bed profiles over first 20 years of experiment. Early profiles are not migrated as flexure proceeds.

conducted a series of global climate model (GCM) experiments using maximum and minimum solar insolation for the northern hemisphere over a Milankovitch cycle involving various partial pressures of CO_2. The model simulations predict arid summers for both maximum and minimum insolations, but considerably wetter winters for the case of maximum insolation. Their results support the hypothesis (Barron et al., 1985) that limestone-marl sequences in the Western Interior Seaway reflect variations in rainfall and runoff from the continental interior. We think it is also likely that these climatic variations affected rates of clastic sediment production and ultimately progradational events.

Experiment 7-12: River Progradation with Variable Sediment Supply

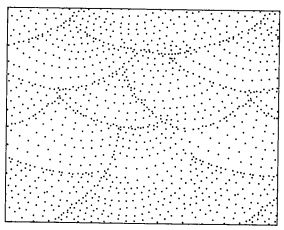

To start simply, we keep the same initial and boundary conditions as Experiment 7-10, but turn off sea level changes and turn on sediment feed changes. The latter varies according to the function (expressed in FORTRAN notation):

$$\text{FEED} = \text{MFEED} + 50.0*\text{DSIN}(6.28319*\text{NT}*\text{DELT}/\text{T}) \qquad (7\text{-}10)$$

where T is the same as in Experiment 7-8.

Results presented as a surface (Figure 7-14) and a contour plot (Figure 7-15) of bed elevation, where the x axis is distance downstream and the y axis is time, show that varying the sediment feed causes cut-and-fill cycles similar to those produced by varying sea level, although there are distinct differences. Maximum cut and fill in Experiment 7-12 occurs upstream, not downstream. The episodes of cutting and filling sweep downstream through time, as might be expected where the cause is upstream. In the first 30 km, the depth of incision when sedi-

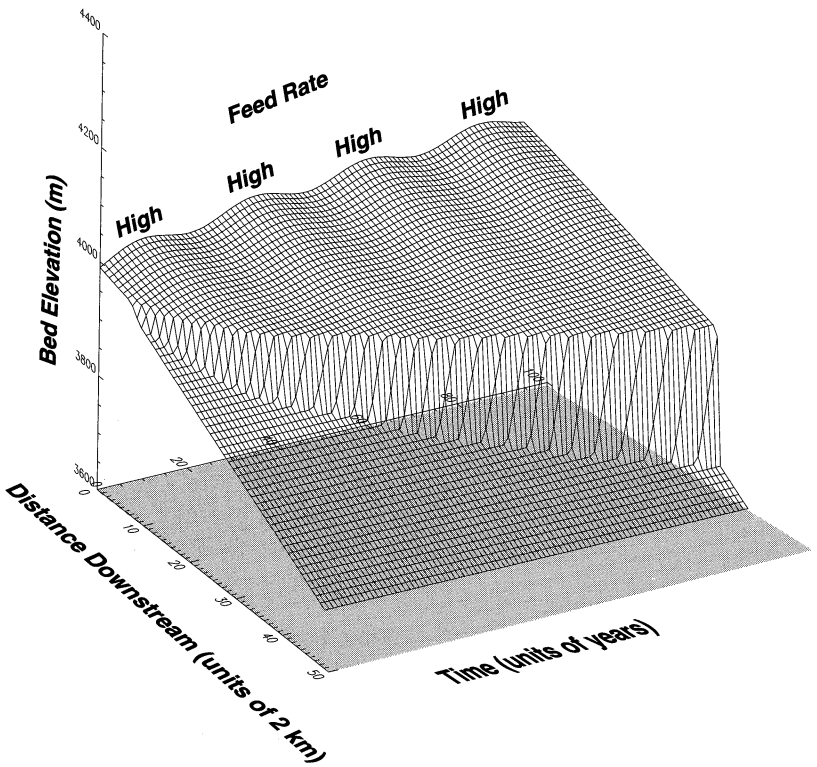

Figure 7-14
Model results for Experiment 7-12 showing time lines through fluvial and deltaic sediments for constant eustatic sea level, temporally varying sediment feed, and no flexure.

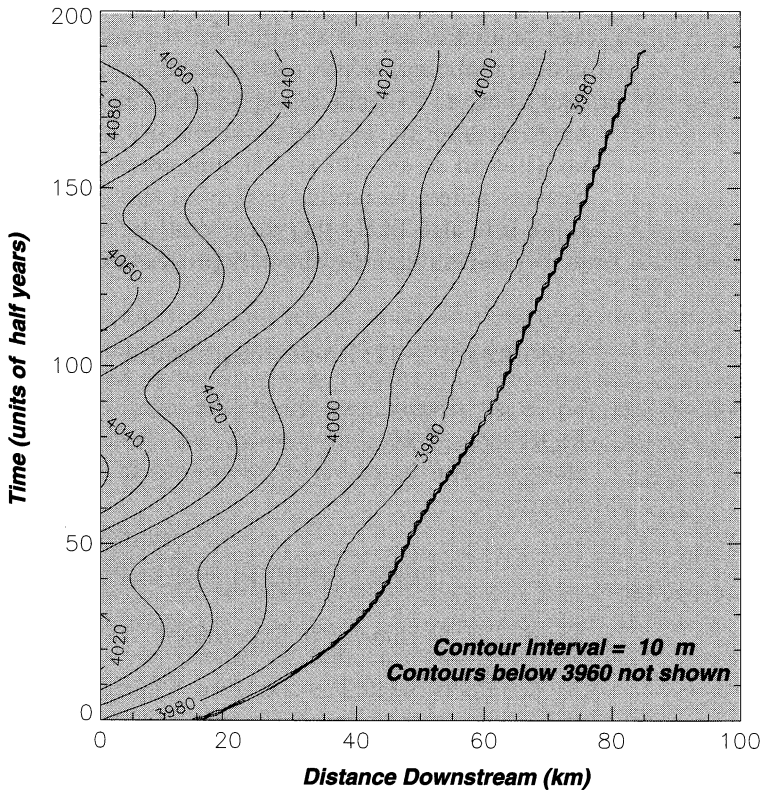

Figure 7-15 Contour plot of space-time surface for Experiment 7-12.

ment feed is low is on the order of 5 m. In this example, the rate of alluviation is so high and the continental shelf is so steep that the stream cuts into its own deposits (Figure 7-16). However, we could conceive of a case where the stream incises into the underlying shelf sediments over a downstream distance of tens of kilometers, producing the stratigraphy of Figure 7-8.

CONCLUDING STATEMENT

What have we accomplished in this book? We have tried to show that some important geologic processes that govern the evolution of sedimentary basins can be represented by first principles derived from physics. This has been done at a price, for we have omitted biological components and mostly ignored the gross influences of plate tectonics. But, the physical principles that underlie the processes presented here are firmly established in science, and we can be confident that they apply broadly in geology. Since the world overall is much too large to treat as a whole, we have focused on sedimentary basins, but the processes apply elsewhere, a point we hope our readers appreciate.

When processes are broken down into their physical components, they can be represented by equations. The substantial space that we devote to equations is justified, we suggest, because we lack effective alternate means for representation. Relationships are often more difficult to represent in words or drawings. An additional advantage of equations is that they can be solved by computers when placed

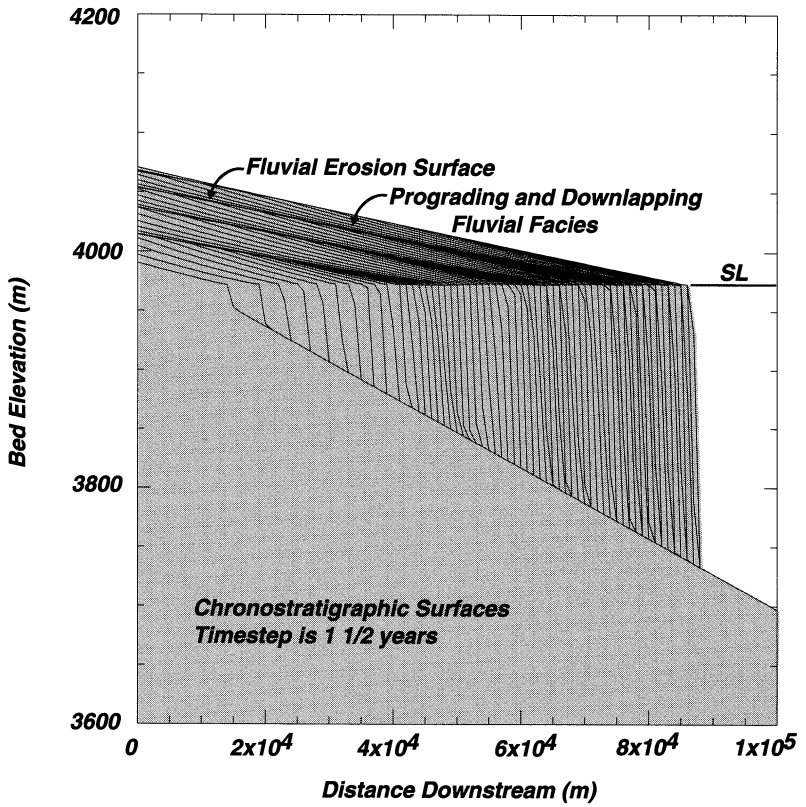

Figure 7-16 Modeled cross section of chronostratigraphic surfaces resulting from boundary conditions of Experiment 7-12.

in finite difference form, and the numerical solutions obtained can be displayed in graphs and maps whose forms are familiar to geologists.

Perhaps most importantly, we have tried to show that geologic processes act in concert with one another. All are components of the dynamic system represented by the earth as a whole. No process operates independently, with every process affecting every other process to a degree, whether large or small. Geologists need to interpret the earth as a dynamic system, and they need the tools to do so. In our limited way, we have tried to provide these tools as representations of processes, and we have tried to show how these processes can be linked in systems in which alternative assumptions can be tested in simulation experiments.

Our representations of processes involve only two dimensions, either as vertical sections or two geographic dimensions. This is a shortcoming, of course, because the world exists in three dimensions. On the other hand, two dimensions are much simpler to represent than three, dictating that our formulations be confined to two dimensions in light of the book's introductory nature.

What will this effort accomplish? We hope it will convince geologists that their science is as beholden to first principles as the other physical sciences. Furthermore, it may stimulate the extension to three dimensions, where the physical principles are the same but the implementation is harder.❖

Notation

Chapter 1

$\dot{e}$ = erosive flux off wedge surface

H = thickness of material entering toe

h = height of wedge surface above vertex

V = convergence velocity

α = topographic slope

β = basal slope of wedge

Ψ_o and Ψ_b = acute angles between axes of principal compressive stress (σ_1) and topographic and basal surfaces, respectively

Chapter 2

a_2 = thickness of column composed of air

c_1 = thickness of column composed of crust

c = distance in Green's function solution

D = flexural rigidity

E = Young's modulus

g = acceleration of gravity

h = elastic thickness of beam

K = relative density

M = moment acting on plate segmentpn

m_1 = thickness of column composed of mantle

n = Poisson's ratio

P = horizontal force acting on plate segment

$q(x)$ = downward force per unit area

V = net shear force that acts on cross section of plate in vertical direction

w = thickness of column of water

w = deflection of plate

ε = distance in Green's function solution

ρ_{air} = density of air

ρ_c = density of crust

ρ_m = density of mantle

ρ_w = density of water

σ_L = magnitude of stress in lithosphere induced by flexure

λ = restoring force

Chapter 3

A = drainage basin area

$A(x)$ = catchment area

$B(x,y,t)$ = mass of earth material passing from one cell to a neighbor per unit time per unit cell width

$D_s$mean denudation rate in meters per thousand years

D_x = diffusion coefficient (units of kg $m^{-1}s^{-1}$) in x direction

dx = cell dimension in x direction

dy = cell dimension in y direction

g = gravitational acceleration

H = elevation in km

$h(x,y)$ = height of each cell in landscape model

i_b = immersed-weight sediment transport rate per unit flow width

k = dimensionless proportionality constant

M = number of nodes in y direction

M_s = suspended sediment load

m = exponent

N = number of nodes in x direction

n = exponent

p = rainfall rate

q = water discharge per unit flow width

Q_s = suspended and bedload sediment discharge

$Q(x,t)$ = total river discharge

$q(x,t)$ = volume per unit time per unit of downstream length

$q_s(x,t)$ = rate of addition of sediment to a stream per unit stream length

$q_s(x,y,t)$ = mass transfer among cells of sediment and dissolved load in stream channels

R = mean relief in basin in meters

$R(x,y,t)$ = rate of mass addition to each cell due to tectonic thickening

S = the energy slope of the stream

t = time(s)

U = uplift rate

ρ = density of the fluid

σ = bulk density of cell

Chapter 4

A = pivot point

A = cross-sectional flow area

A' = constant in the Bridge and Dominic bed velocity equation

A_L = area of grains exposed to lift per unit bed area

a = coefficient of drag

a = fractional constant in entrainment analysis

a = height of the moving bed layer

a_f = moment arm in entrainment analysis

a_g = moment arm in entrainment analysis

B = empirical constant used in the suspension inequality

b = flow width

C = Chezy constant

C_D = coefficient of drag

C_g = center of gravity of a grain

C_{ij} = local suspended sediment concentration of grain size i of the mineral density j

C_L = coefficient of lift

c = constant

D = flow depth

D_* = dimensionless grain diameter

D_{50} = mean grain diameter of the active layer

D_{ij} = grain diameter of grain size fraction i of the mineral density j

D_{nij} = nominal grain diameter of grain size fraction i of the mineral density j

E = specific energy

e = smallest instantaneous shear stress greater than τ_{cij}

F = fluid force

F_{TL} = turbulent lift force on the bedload per unit bed area

f = largest instantaneous shear stress less than or equal to τ_{sij}

G = grain submerged weight

g = gravitational acceleration

H_T = total head

i_b = bedload transport rate per unit width

K = constant in bedload transport equation

k = characteristic bed roughness

k_M = coefficient in Manning's equation = 1 $m^{1/2}s^{-1}$

m = coefficient in the Komar entrainment function

n = Manning's roughness coefficient

P = protrusion height

P_k = proportion of time the kth shear stress interval is active

p = bed porosity

p = fluid pressure at a point along a streamline

Q = flow discharge

R = hydraulic radius (m)

Re_D = grain Reynolds number

S_f = friction slope

S_s = width integrated suspended load transport rate

S_o = bed slope

s = distance along an axis

T = torque in entrainment analysis

T_a = the active layer thickness

t = time (s)

U_{bij} = the near bed velocity of grain size i of the mineral density j

U_{*cij} = critical shear velocity necessary to entrain grain size i of mineral density j

U''_* = skin friction component of the mean, time averaged bed shear velocity

V = mean flow velocity

V_c = critical mean flow velocity

V_x, V_y, V_z, V_s=fluid velocity along the x, y, z and s axes respectively

$V(z)$ = velocity as a function of depth

W_{ij} = volumetric proportion of grain size interval i of mineral density j in the active layer

W_* = dimensionless settling velocity

W' = grains' immersed weight per unit bed area

w_{ij} = settling velocity of grain size interval i of mineral density j

x = distance along an axis parallel to the bed in the flow direction

y = flow depth

y = distance along an axis parallel to the bed in the cross flow direction

z = distance normal to the bed

z_{bij} = bed elevation attributable to the ith grain size fraction of mineral density j(m)

α = pivot angle in entrainment analysis

α = bed slope angle

$\tan \alpha'$ = a dynamic friction coefficient in the modified Bagnold equation

γ = fluid specific gravity

ε_z = eddy viscosity at a height z above the bed

ζ = angle of fluid force vector with horizontal in entrainment analysis

Θ_c = dimensionless bed shear stress

Θ_{cij} = dimensionless critical shear stress necessary to entrain grain size i of mineral density j

$\Theta_{c_{50}}$ = dimensionless critical shear stress necessary to entrain the mean grain diameter

κ = von Karman's constant

ν = kinematic fluid viscosity

ν' = root mean squares of upward and downward turbulent fluctuations

ρ = fluid density

σ_j = mineral density j

σ_t = standard deviation of the shear stress distribution

τ = instantaneous shear stress

τ_{cij} = critical shear stress necessary to entrain grain size i of mineral density j

$\tau_{c_{50}}$ = critical shear stress necessary to entrain the mean grain diameter

τ_o = skin friction component of the time averaged, mean bed shear stress

τ_{sij} = the minimum shear stress necessary to suspend grain size i of mineral density j

Φ = weighting factor for the Preissman difference scheme

ϕ = grain pivot angle

subscripts and superscripts

a = at height a above the bed

b = bedload

i = grain size interval i

j = mineral density j

k = shear stress interval number k

1 = node number 1

z = at height z above the bed

$''$ = skin friction component

A = area over which bedload is spread, here assumed to be given by width of river mouth times x_o

$$a = \frac{\sqrt{\pi} C_1}{2}$$

a = wave amplitude

b_o = channel width at river mouth

C_1 = 0.109

$$C_o = \sqrt{g\,(h+\varsigma)}$$

c = celerity of shallow water wave

cosh = hyperbolic cosine

D = transport coefficient

f = Coriolis parameter

g = gravitational acceleration

H = known elevation

$H_{o_{(1/3)}}$ = deep water significant wave height in meters

h = bed elevation

h = water depth

i = current cross section or node number

k = friction coefficient

k = wave number, equal to $2\pi/L$

$$L = T\sqrt{g\,(h+\varsigma)}$$

n = unit outward vector

n = current timestep

p = fluid pressure

p = normal pressure (760 mm of mercury) minus central pressure of hurricane in mm of mercury

p_n = pressure at outskirts of storm

p_o = central pressure

Q_b = bedload transport rate

Q_o = river discharge at river mouth

Q_s = suspended load at river mouth

R = radial distance from storm center to region of maximum wind speed

$R^k_{i,j}$ = amount of increase in elevation over next timestep Δt due to other processes such as hemipelagic sedimentation

T_s = significant wave period in seconds

t = time

U_{max} = maximum gradient wind speed 10 meters above water surface calculated from (5-109) and (5-110) when $r = R$

U_R = maximum sustained windspeed in meters per second, calculated for 10 meters above mean sea surface at radius R

$U_{SM}(r)$ = term added vectorially to wind velocity at each value of r

U_* = shear velocity

u_o = flow velocity at river mouth

$u_{x,y}$ = longitudinal velocity

u and w = x- and z-directed fluid velocities

V_F = forward speed of hurricane in meters per second

V_F = velocity of storm center

W = wind speed measured 10 m above sea surface

x = distance

z_o = roughness length

$$\alpha = \sqrt{\frac{1}{C_1\sqrt{\pi}}}$$

α = coefficient depending upon forward speed of a hurricane; for slowly moving hurricane, $\alpha = 1.0$

α = proportion of river bedload deposited beyond delta topset beds

γ = specific gravity of water

Δt = finite timestep

Δx = finite space step

$\delta = 0.67 \times 10^{-5}$ ft^{-1}

$\theta_x = D_x\Delta t/(2(\Delta x)^2)$

$\theta_y = D_y\Delta t/(2(\Delta y)^2)$

κ = von Karman's constant (equal to 0.4 for clear water)

ρ = fluid density

ρ_a = air density

ρ_b = bulk density of deposited bedload

ρ_{bs} = bulk density of s size fraction in kg m^{-3}

$\varsigma_{r_1}^{n+1}$ = predicted water surface elevation of reflected waves at new timestep

$\varsigma_{r_1}^{n}$ = water surface elevation due to reflected waves at node 1

$\varsigma_{r_2}^{n}$ = water surface elevation due to reflected waves at node 2

σ = standard deviation of Gaussian velocity distribution

σ = wave angular frequency, equal to $2\pi/T$

Φ = velocity potential

ϕ = angle of latitude

Ω = angular velocity of earth's rotation (of magnitude 2π radians per sidereal day or 7.29×10^{-5}rad s^{-1})

A = cross-sectional area of column in m^2

h = total hydraulic head in m

g = acceleration of gravity in m/s^2

K = proportionality factor that depends on properties of both porous material and fluid in column in m/s

k = index of layer that loads sediment column

k_x = intrinsic permeability in x direction in m^2

f_h = anisotropy coefficient for horizontal direction (which is usually 1)

f_v = anisotropy coefficient for vertical direction (which is usually < 1)

L = length of column in m

n = number of columns in grid

V_p = pore volume in m^3

u_s = velocity of solid material in m/s

p = pressure in Pa (pascals)

p_0 = reference pressure in Pa

Q = volume of water flowing through column in m

q = volume flux in m^3/s

q_z = volume flux in the vertical direction in m^3/s

S = sediment load in Pa

V = bulk volume in m^3

V_p = pore volume in m^3

z = thickness in m

z = elevation in m

z_{oj} = elevation of topography

α = soil compressibility in Pa^{-1}

β = fluid compressibility in Pa^{-1}

Δh = difference in hydraulic head between top and bottom of column in m

μ = dynamic viscosity in cP (centipoises) or Pa

v_s = true solid velocity in m/s

v_w = true fluid velocity in m/s

ρ_s = sediment density in kg/m^3

ρ_w = water density in kg/m^3

σ = total stress in Pa

σ_e = effective stress in Pa

ϕ = porosity

AMP = amplitude of variation

b = width of active bed, assumed to be equal to flow width

D = grain diameter

$i_{b_{ik}}$ = bedload transport rates of ith-jth fraction (kg s^{-3})

jn = node number

m = maximum number of nodes

p = bed porosity

Q_{in} = amount of lateral sediment feed at node jn that enters over timestep Δt,

q = water discharge

q_s = rate at which sediment enters river bed from beneath as consequence of uplift

$S_{s_{ik}}$ = suspended load transport rates of ith-jth fraction (kg s^{-1})

T = period (50 years)

W = stream width

WSEBC = water surface elevation boundary condition at control node

WSEBCB = mean water level

x = distance traveled

$z_{b_{ik}}$ = bed elevation attributable to ith-jth bed fraction

β = comminution coefficient in terms of fraction lost per unit distance traveled

σ_j = density of jth grain species